Attitude, body-fixed Earth rotation rate, and sensor bias estimation using single observations of direction of gravitational field

Joel Reis, Pedro Batista, Paulo Oliveira, and Carlos Silvestre

Automatica, vol. 125, 109475, March 2021

https://doi.org/10.1016/j.automatica.2020.109475

Attitude, body-fixed Earth rotation rate, and sensor bias estimation using single observations of direction of gravitational field

Joel Reis [a], Pedro Batista [b], Paulo Oliveira [b,c], Carlos Silvestre [a,b]

[a] *Faculty of Science and Technology, University of Macau, Taipa, Macao.*

[b] *Institute for Systems and Robotics, Instituto Superior Técnico, Universidade de Lisboa, Lisboa 1049-001, Portugal.*

[c] *LAETA—Associated Laboratory for Energy, Transports and Aeronautics, IDMEC—Institute of Mechanical Engineering, Instituto Superior Técnico, Universidade de Lisboa, Lisboa 1049-001, Portugal.*

Abstract

This paper addresses the problem of estimating the attitude of a robotic platform using biased measurements of: i) the direction of the gravitational field and ii) angular velocity obtained from a set of high-grade gyroscopes sensitive to the Earth's rotation. A cascade solution is proposed that features a Kalman filter (KF) tied to a rotation matrix observer built on the special orthogonal group of order 3. The KF, whose model stems from a uniformly observable linear time-varying system, yields estimates of: i) the Earth's total rotational rate; ii) two sensor biases associated with the aforementioned measurements; and, iii) noise-filtered and bias-corrected accelerometer data. All estimates are expressed in the platform's body-fixed frame. In turn, the attitude observer put forward is shown to be almost globally asymptotically stable, in particular locally input-to-state stable with respect to the KF errors. Experimental results are showcased that successfully demonstrate the efficiency of the proposed attitude estimation solution.

Keywords: Nonlinear observer and filter design; guidance navigation and control.

1 Introduction

At its core, the problem of dynamic attitude estimation aims to describe the rotational motion of a rigid body with respect to a given frame of reference. Inspiring the continuous development of attitude estimation solutions is not only a pursuit of computationally lighter algorithmic implementations, but also a recurrent need to overcome well-known topological obstructions [1], the intrinsic limitations of low-cost strapdown sensors [2], [3], and/or a need to deal with circumstances where particular sensors are deemed unreliable, for instance, the global positioning system (GPS) in underwater domains, or magnetometers in environments with strong magnetic signatures.

Aware of these pitfalls, the scientific community, in a particular attempt to simplify setup designs, has been actively exploring solutions that resort to single vector observations, see, e.g., [4], [5], [6], and references therein. Moreover, to be able to simultaneously determine sensor biases, in particular concerning gyroscopes, is crucial in order to avoid accumulation of errors, which, if unattended, may compromise feasibility. Among the extensive literature on this latter subject, the reader is referred to, e.g., [7] and [8].

Gradually, the advent of high-grade sensors, such as fiber optic gyroscopes (FOGs) [9], opened the door for a new class of attitude observers focused on applications where high accuracy is a key demand, for instance, in the determination of true north for gyro-compass-based applications, see [10], [11], and references therein.

This work, by assuming that the gyroscopes are sensitive to the rotation of the planet, proposes a strategy for attitude determination of robotic platforms with simultaneous estimation of the Earth's angular velocity and sensor offsets. Alternatively to more conventional approaches, which make use of the celebrated nonlinear complimentary filter, as seen in [12] and [13], this paper introduces a cascade routine that features a Kalman filter (KF) whose estimates are fed to a rotation matrix observer built on the special orthogonal group of order three. Resorting to single observations of the direction of the gravitational field, and to implicit knowledge of the Earth's spin about its own axis, the KF is able to estimate two sensor biases and the Earth's total angular velocity, in addition to filter out noise from accelerometer data. The Kalman stage is followed then by a rotation matrix observer that is shown to be almost globally asymptotically stable (AGAS), in particular locally input-to-state stable (LISS) with respect to the errors of the KF, which converge asymptotically to zero.

Previous works by the authors, see references [14], [15], [16], [17], [18], have been tackling, from different viewpoints, the problem of true-north attitude determination, although without considering biases over the measurements, which is a considerably less challenging setting from a theoretical perspective. In particular, the works in [16] and [17] propose a strategy where the angular velocity of the planet is only implicitly estimated, which greatly simplifies the structure of the observers, although at the expense of convergence times and stability guarantees. The techniques in [14] and [15] showcase two cascade solutions where the angular velocity of the planet is explicitly estimated; global stability is guaranteed if topological relaxations are considered. More recently, in [18], a discrete-time version of the problem is studied that illustrates

⋆ Corresponding author C. Silvestre.

Email addresses: joelreis@um.edu.mo (Joel Reis), pbatista@isr.tecnico.ulisboa.pt (Pedro Batista), paulo.j.oliveira@tecnico.ulisboa.pt (Paulo Oliveira), csilvestre@um.edu.mo (Carlos Silvestre).

the benefits of a Kalman based implementation; the adaptive nature of the Kalman gain helps to circumvent an otherwise cumbersome, empirical gain tuning process, often leaning on sets of piecewise constant gains.

It should be stressed that whereas the vast majority of attitude estimation solutions available in the literature require explicit measurements of at least two inertial reference vectors, in this paper, as well as in the work of Spielvogel et al. [11], only one inertial reference vector needs to be explicitly measured. Furthermore, the sole reference vector is assumed to be constant, therefore bypassing the need to require the system to satisfy a persistency of excitation condition.

In this paper, the source of reference observations is restricted to the accelerometer case, with the relationship between the direction of the gravitational field and the Earth's angular velocity being geometrically exploited for the purpose of system design simplifications. As opposed to the work in [11], which examines this same relationship, herein a transition matrix is computed that offers a better insight into the set of trajectories that undermine the observability of the system. Moreover, the overall performance, validated with both simulation and experimental results, is much faster than the one shown in [11].

The rest of the paper is organized as follows: in Section 2, an overview of the problem statement is sketched followed by the design of a linear time-varying (LTV) system and ensuing KF application. The observability of this LTV system is also analyzed. Section 3 is dedicated to the main result of the paper, where a proposed attitude observer is shown to be LISS with respect to the errors of the KF. Section 4 showcases a set of experimental results that demonstrate the efficiency of the proposed attitude estimation solution. Finally, Section 5 elaborates upon a few conclusions and discussions.

1.1 Notation

Throughout the paper, a bold symbol stands for a multi-dimensional variable, the symbol $\mathbf{0}$ denotes a matrix of zeros and $\mathbf{I}$ an identity matrix, both of appropriate dimensions. The exponential of a matrix is denoted by $\exp(\cdot)$. A positive definite matrix $\mathbf{M}$ is denoted by $\mathbf{M} \succ \mathbf{0}$. The set of unit vectors on $\mathbb{R}^3$ is denoted by $S(2)$. The special orthogonal group of order three is denoted by $SO(3) := \{\mathbf{X} \in \mathbb{R}^{3\times 3} : \mathbf{X}\mathbf{X}^\mathsf{T} = \mathbf{X}^\mathsf{T}\mathbf{X} = \mathbf{I} \wedge \det(\mathbf{X}) = 1\}$. The skew-symmetric matrix of a vector $\mathbf{a} \in \mathbb{R}^3$ is defined as $\mathbf{S}(\mathbf{a})$, such that given another vector $\mathbf{b} \in \mathbb{R}^3$ one has (the cross-product) $\mathbf{a} \times \mathbf{b} = \mathbf{S}(\mathbf{a})\mathbf{b}$. Orthogonality between vectors is represented by the symbol $\perp$. Finally, for convenience, the transpose operator is denoted by the following superscript $(\cdot)^\mathsf{T}$, and the trace function by $\mathrm{tr}(\cdot)$.

2 Earth velocity and bias estimation

2.1 Problem Statement

Consider a robotic platform describing a 3D rotational motion in a dynamic environment. Suppose that the platform is equipped with a set of three high-grade, orthogonally mounted rate gyros that are accurate enough to perceive the angular velocity of the planet. In addition, let the platform also be equipped with a set of tri-axial accelerometers. Consider also two frames, one inertial and another fixed to the platform's body. As convincingly argued in [13], for low frequency response, the gravitational field often dominates the body acceleration, meaning that one can assume the accelerometer measurements are constant when expressed in the inertial coordinate frame.

The key goal is thus to determine the rotation matrix from the body frame to the inertial one using biased angular velocity readings from the high-grade FOGs, which implicitly measure the speed of Earth's spin, in addition to biased body-fixed measurements of the gravitational field. As a by-product, the two offsets associated with the measurements, as well as the Earth's rotation rate expressed in $\{B\}$, are explicitly estimated.

2.2 Linear time-varying system design

Let $\mathbf{R}(t) \in SO(3)$ denote the rotation from a body-fixed frame $\{B\}$ to a local inertial coordinate reference frame $\{I\}$ [*]. In this work, both frames follow the North East Down (NED) coordinate frame convention, with the origin of $\{B\}$ located at the body's center of gravity.

The derivative of $\mathbf{R}(t)$ with respect to time obeys

$$\dot{\mathbf{R}}(t) = \mathbf{R}(t)\mathbf{S}[\boldsymbol{\omega}(t)], \tag{1}$$

where $\boldsymbol{\omega}(t) \in \mathbb{R}^3$ is the angular velocity of $\{B\}$ with respect to $\{I\}$, expressed in $\{B\}$. The measurements collected from the high-grade FOGs, denoted by $\boldsymbol{\omega}_m(t) \in \mathbb{R}^3$, are given by

$$\boldsymbol{\omega}_m(t) = \boldsymbol{\omega}(t) + \boldsymbol{\omega}_E(t) + \mathbf{b}_{\boldsymbol{\omega}} + \mathbf{n}_{\boldsymbol{\omega}}(t), \tag{2}$$

where $\boldsymbol{\omega}_E(t) \in \mathbb{R}^3$ is the angular velocity of the Earth about its own axis, expressed in $\{B\}$, $\mathbf{b}_{\boldsymbol{\omega}} \in \mathbb{R}^3$ is a constant bias offset, and $\mathbf{n}_{\boldsymbol{\omega}}(t) \in \mathbb{R}^3$ corresponds to zero-mean sensor noise, assumed to be additive, white and Gaussian in nature. Let the accelerometer data be denoted by $\mathbf{a}_m(t) \in \mathbb{R}^3$, which correspond to noisy and biased sensor readings of the platform's true linear acceleration $\mathbf{a}(t) \in \mathbb{R}^3$, i.e.,

$$\mathbf{a}_m(t) = \mathbf{a}(t) + \mathbf{b}_{\mathbf{a}} + \mathbf{n}_{\mathbf{a}}(t), \tag{3}$$

where $\mathbf{b}_{\mathbf{a}} \in \mathbb{R}^3$ is a constant bias offset that characterizes the tri-axial accelerometer, and $\mathbf{n}_{\mathbf{a}}(t) \in \mathbb{R}^3$ is assumed to be modeled from an additive, zero-mean, white Gaussian noise distribution. As it is the case with most robotic applications, for low frequency response, the gravitational field, herein denoted by $\mathbf{g}(t) \in \mathbb{R}^3$, often dominates the linear acceleration described by the robotic apparatus [13]. Therefore, consider the approximation

$$\mathbf{a}(t) \approx \mathbf{g}(t). \tag{4}$$

Furthermore, let ${}^I\boldsymbol{\omega}_E, {}^I\mathbf{g} \in \mathbb{R}^3$ be such that, for all $t \geq 0$,

$$\begin{cases} \boldsymbol{\omega}_E(t) = \mathbf{R}^\mathsf{T}(t){}^I\boldsymbol{\omega}_E & \text{(5a)} \\ \mathbf{g}(t) = \mathbf{R}^\mathsf{T}(t){}^I\mathbf{g}. & \text{(5b)} \end{cases}$$

For ease of notation, and because most equations are developed in $\{B\}$, leading superscripts of body-fixed vectors are dropped. Thus, whenever a vector is presented without a leading superscript, that vector is implicitly expressed in $\{B\}$, e.g., $\boldsymbol{\omega}_E \equiv {}^B\boldsymbol{\omega}_E$. Notice that ${}^I\boldsymbol{\omega}_E$ and ${}^I\mathbf{g}$ are both known quantities.

The following assumptions are considered throughout the remainder of the paper.

Assumption 1 *The constant inertial reference vectors ${}^I\boldsymbol{\omega}_E$ and ${}^I\mathbf{g}$ are not collinear, i.e., ${}^I\boldsymbol{\omega}_E \times {}^I\mathbf{g} \neq \mathbf{0}$.*

Assumption 2 *The accelerometer bias is such that $\|\mathbf{b}_{\mathbf{a}}\| << \|\mathbf{g}(t)\| = \|{}^I\mathbf{g}\| = g$, with $g \in \mathbb{R}$ referring to the acceleration of gravity.*

[*] This frame, which rotates along with the Earth's spin, is not exactly inertial, but considered as such for this application because the apparent forces due to the Earth's movement are within the accelerometer's error.

The first assumption concerns stability and is fundamental in the main result of this work. It ensures that unequivocal information on directionality can be extracted from both reference vectors as long as they define a plane. The second assumption is always verified in practice: the accelerometer bias is several orders of magnitude smaller than the acceleration of gravity. As result, the measured acceleration is never zero.

At any given latitude $\varphi \in \mathbb{R}$, the vectorial representation of the Earth's angular velocity in the NED inertial frame is given by ${}^I\boldsymbol{\omega}_E = \left\|{}^I\boldsymbol{\omega}_E\right\| [\cos(\varphi),\, 0,\, -\sin(\varphi)]^\mathsf{T}$. Granted that this inertial vector does not span the East direction, proceed to write $\boldsymbol{\omega}_E(t)$ as the sum of a *North* and a *Down* component, i.e., $\boldsymbol{\omega}_E(t) = \boldsymbol{\omega}_{E,N}(t) + \boldsymbol{\omega}_{E,D}(t)$, where

$$\begin{cases} \boldsymbol{\omega}_{E,N}(t) := \mathbf{R}^\mathsf{T}(t) \left[\left\|{}^I\boldsymbol{\omega}_E\right\| \cos(\varphi),\, 0,\, 0\right]^\mathsf{T} & \text{(6a)} \\ \boldsymbol{\omega}_{E,D}(t) := \mathbf{R}^\mathsf{T}(t) \left[0,\, 0,\, -\left\|{}^I\boldsymbol{\omega}_E\right\| \sin(\varphi)\right]^\mathsf{T}. & \text{(6b)} \end{cases}$$

Observe that the norm of both vectors is constant, and, most noticeably, that the inner product $\boldsymbol{\omega}_{E,N}^\mathsf{T}(t)\boldsymbol{\omega}_{E,D}(t)$ is zero. Similarly, it is a fact that ${}^I\mathbf{g}$ lies solely along the *Down* axis of the NED inertial frame. This, in turn, allows us to write (6b) as

$$\boldsymbol{\omega}_{E,D}(t) = \alpha \mathbf{g}(t) = \alpha \left(\mathbf{a}_m(t) - \mathbf{b}_\mathbf{a}\right), \tag{7}$$

with constant $\alpha := -\left\|\boldsymbol{\omega}_{E,D}\right\| / g < 0$.

Next, take the derivative of (5b), and rewrite the result as

$$\mathbf{0} = \dot{\mathbf{R}}(t) \left(\mathbf{a}_m(t) - \mathbf{b}_\mathbf{a}\right) + \mathbf{R}(t)\dot{\mathbf{g}}(t). \tag{8}$$

For the following derivation, assume noise-free FOG data [†]. Substituting (2) in (1) and using it in (8), noticing that the cross product of parallel vectors is zero, and, finally, isolating the term $\dot{\mathbf{g}}(t)$ yields

$$\dot{\mathbf{g}}(t) = -\mathbf{S}\left[\boldsymbol{\omega}_m(t) - \boldsymbol{\omega}_{E,N}(t) - \mathbf{b}_{\boldsymbol{\omega}}\right] \left(\mathbf{a}_m(t) - \mathbf{b}_\mathbf{a}\right). \tag{9}$$

Following through a similar process, compute the derivative of (6a), which, in view of equation (7), may be rewritten as

$$\dot{\boldsymbol{\omega}_{E,N}}(t) = -\mathbf{S}\left[\boldsymbol{\omega}_m(t) - \alpha\left(\mathbf{a}_m(t) - \mathbf{b}_\mathbf{a}\right) - \mathbf{b}_{\boldsymbol{\omega}}\right] \boldsymbol{\omega}_{E,N}(t). \tag{10}$$

To be able to design an LTV system, a few approximations must now be carried out. Start by rewriting (9) as

$$\begin{aligned} \dot{\mathbf{g}}(t) = &-\mathbf{S}\left[\boldsymbol{\omega}_m(t)\right] \left(\mathbf{a}_m(t) - \mathbf{b}_\mathbf{a}\right) \\ &+ \mathbf{S}\left[\boldsymbol{\omega}_{E,N}(t) + \mathbf{b}_{\boldsymbol{\omega}}\right] \left(\mathbf{a}_m(t) - \mathbf{b}_\mathbf{a}\right), \end{aligned} \tag{11}$$

and notice that the term $\boldsymbol{\omega}_{E,N}(t) + \mathbf{b}_{\boldsymbol{\omega}}$ is always very small [‡]. Consequently, since, according to *Assumption* 2, $\|\mathbf{b}_\mathbf{a}\| << \|\mathbf{a}_m(t)\|$, one may assume that $\mathbf{S}\left[\boldsymbol{\omega}_{E,N}(t) + \mathbf{b}_{\boldsymbol{\omega}}\right] \mathbf{b}_\mathbf{a} \approx \mathbf{0}$. Likewise, in equation (10), since the magnitude of $\mathbf{b}_{\boldsymbol{\omega}}$ is typically within the noise associated with the measurements $\boldsymbol{\omega}_m(t)$, and by invoking once again *Assumption* 2, one may also assume that $\mathbf{S}\left[\alpha\mathbf{b}_\mathbf{a} - \mathbf{b}_{\boldsymbol{\omega}}\right] \boldsymbol{\omega}_{E,N}(t) \approx \mathbf{0}$. In other words, these mild assumptions state, as also discussed in [11], that, in practice, the cross products between sensor biases, and between each bias and the *North* component of the Earth's angular velocity are orders of magnitude smaller than the magnitude of the other vectors. Hence, equations (11) and (10) can be simplified as

$$\dot{\mathbf{g}}(t) \approx -\mathbf{S}\left[\boldsymbol{\omega}_m(t) - \boldsymbol{\omega}_{E,N}(t) - \mathbf{b}_{\boldsymbol{\omega}}\right] \mathbf{a}_m(t) + \mathbf{S}\left[\boldsymbol{\omega}_m(t)\right] \mathbf{b}_\mathbf{a} \tag{12}$$

and

$$\dot{\boldsymbol{\omega}}_{E,N}(t) \approx -\mathbf{S}\left[\boldsymbol{\omega}_m(t) - \alpha\mathbf{a}_m(t)\right] \boldsymbol{\omega}_{E,N}(t), \tag{13}$$

respectively. Finally, the inner product of (7) and $\boldsymbol{\omega}_{E,N}(t)$ helps writing a constraint which will be convenient for the KF implementation. Specifically, one has

$$0 = \boldsymbol{\omega}_{E,N}^\mathsf{T}(t) \left(\mathbf{a}_m(t) - \mathbf{b}_\mathbf{a}\right) \approx \boldsymbol{\omega}_{E,N}^\mathsf{T}(t)\mathbf{a}_m(t). \tag{14}$$

It is important to stress that, as long as *Assumption* 2 holds, and because the Earth's rotational speed is a very small, immutable value, the simplifications carried out in (12), (13), and (14) pose no practical limitations.

Let $\mathbf{x}(t) := [\mathbf{g}^\mathsf{T}(t),\, \boldsymbol{\omega}_{E,N}^\mathsf{T}(t),\, \mathbf{b}_\mathbf{a}^\mathsf{T},\, \mathbf{b}_{\boldsymbol{\omega}}^\mathsf{T}]^\mathsf{T} \in \mathbb{R}^{12}$ denote a system state vector. In the absence of sensor noise, a general LTV system can be formulated as

$$\begin{cases} \dot{\mathbf{x}}(t) = \mathbf{A}(t)\mathbf{x}(t) + \mathbf{B}(t)\mathbf{u}(t) \\ \mathbf{y}(t) = \mathbf{C}(t)\mathbf{x}(t) \end{cases}, \tag{15}$$

where $\mathbf{A}(t) = \left[\begin{array}{cc|c} \mathbf{0} & \mathbf{0} & \\ \mathbf{S}\left[\mathbf{a}_m(t)\right] & \mathbf{S}\left[\boldsymbol{\omega}_m(t) - \alpha\mathbf{a}_m(t)\right] & \mathbf{0} \\ -\mathbf{S}\left[\boldsymbol{\omega}_m(t)\right] & \mathbf{0} & \\ \mathbf{S}\left[\mathbf{a}_m(t)\right] & \mathbf{0} & \end{array}\right]^\mathsf{T} \in \mathbb{R}^{12\times 12}$, $\mathbf{B}(t) = [\mathbf{S}[\boldsymbol{\omega}_m(t)],\, \mathbf{0}]^\mathsf{T} \in \mathbb{R}^{12\times 3}$, $\mathbf{u}(t) \equiv \mathbf{a}_m(t)$, $\mathbf{y}(t) = [\mathbf{a}_m^\mathsf{T}(t),\, 0]^\mathsf{T} \in \mathbb{R}^4$, and, finally, $\mathbf{C}(t) = \begin{bmatrix} \mathbf{I} & \mathbf{0} & \mathbf{I} & \mathbf{0} \\ \mathbf{0} & \mathbf{a}_m^\mathsf{T}(t) & \mathbf{0} & \mathbf{0} \end{bmatrix} \in \mathbb{R}^{4\times 12}$. Notice that the zero element of $\mathbf{y}(t)$ corresponds to a virtual null measurement, which, as seen from (14), acts as a constraint on the LTV system (15).

2.3 Kalman filter implementation

Let the comprehensive system state estimate be denoted as $\hat{\mathbf{x}}(t) := [\hat{\mathbf{g}}^\mathsf{T}(t),\, \hat{\boldsymbol{\omega}}_{E,N}^\mathsf{T}(t),\, \hat{\mathbf{b}}_\mathbf{a}^\mathsf{T}(t),\, \hat{\mathbf{b}}_{\boldsymbol{\omega}}^\mathsf{T}(t)]^\mathsf{T} \in \mathbb{R}^{12}$. A classic KF for the LTV system (15) is thus given by

$$\begin{cases} \dot{\hat{\mathbf{x}}}(t) = \mathbf{A}(t)\hat{\mathbf{x}}(t) + \boldsymbol{\mathcal{K}}(t)\left(\mathbf{y}(t) - \mathbf{C}(t)\hat{\mathbf{x}}(t)\right) & \text{(16a)} \\ \boldsymbol{\mathcal{K}}(t) = \mathbf{P}(t)\mathbf{C}^\mathsf{T}(t)\boldsymbol{\mathcal{R}}^{-1} & \text{(16b)} \\ \dot{\mathbf{P}}(t) = -\mathbf{P}(t)\mathbf{C}^\mathsf{T}(t)\boldsymbol{\mathcal{R}}^{-1}\mathbf{C}(t)\mathbf{P}(t) + \\ \qquad\qquad + \mathbf{A}(t)\mathbf{P}(t) + \mathbf{P}(t)\mathbf{A}^\mathsf{T}(t) + \boldsymbol{\mathcal{Q}}, & \text{(16c)} \end{cases}$$

where $\boldsymbol{\mathcal{Q}} \in \mathbb{R}^{12\times 12}$, $\boldsymbol{\mathcal{Q}} \succ \mathbf{0}$, and $\boldsymbol{\mathcal{R}} \in \mathbb{R}^{4\times 4}$, $\boldsymbol{\mathcal{R}} \succ \mathbf{0}$, are the covariance matrices of the process and observation noises, respectively. Each of these two matrices, herein assumed constants, depicts a different additive white Gaussian noise distribution, and can be seen as tuning knobs. Note that, in the presence of sensor noise, the premises on which the KF is built are no longer rigorous, since matrices $\mathbf{A}(t)$, $\mathbf{B}(t)$, and $\mathbf{C}(t)$ become sources of multiplicative noise, therefore overruling claims of optimality. This trait, in addition to the approximations conducive to equations (12) and (13), better characterize the KF (16) as sub-optimal. Handling cross-correlated sensor noises is out of the scope of this work, but the interested reader can find results on this topic, for instance, in [19, Section 9.5] and in [20], among several others.

[†] Note that this is not an approximation. The evolution in time of a physical quantity describes a property of the system, which can be measured but is independent of sensors.

[‡] All recent commercially available FOGs, designed specifically for fast and accurate navigation purposes, guarantee levels of bias instability below 1 (deg/h). Therefore, even in the worst case scenario, it would follow that $\|\boldsymbol{\omega}_{E,N}(t) + \mathbf{b}_{\boldsymbol{\omega}}\| \lessapprox 10^{-4}$ (rad/s) for all $t \geq 0$.

At last, using the output of the KF (16), i.e., $\hat{\mathbf{x}}(t)$, allows us to reconstruct an estimate of the Earth's total angular velocity as $\hat{\boldsymbol{\omega}}_E(t) = \hat{\boldsymbol{\omega}}_{E,N}(t) + \alpha\hat{\mathbf{g}}(t)$.

2.4 Observability Analysis

The observability of the problem of attitude estimation with biased measurements is studied in this section.

It is well-known that a KF can be designed to be asymptotically stable if certain observability criteria are met [21]. In particular for the LTV system (15), globally exponentially stable error dynamics can be attained.

The following theorem reports an observability condition which, if verified, renders the LTV system (15) observable. This condition is shown to be simultaneously necessary and sufficient.

Theorem 3 *The LTV system* (15) *is observable on* $\mathcal{T} := [t_0, t_f]$ *if and only if*

$$\exists_{\substack{t_1\in\mathcal{T}\\ c_1,c_2\in\mathbb{R}\setminus\{0\}}} \quad c_1\mathbf{a}_m(t_0)\times\mathbf{a}_m(t_1) + c_2\boldsymbol{\omega}_m(t_0)\times\boldsymbol{\omega}_m(t_1) \neq \mathbf{0}. \tag{17}$$

and if, for some constant vector $\mathbf{v}\in\mathbb{R}^3$, $\mathbf{v}\perp\mathbf{a}_m(t_0)$,

$$\exists_{t_1\in\mathcal{T}} \quad \mathbf{v}^\mathsf{T}\exp\left(\mathbf{S}\left[\int_{t_0}^{t_1}\boldsymbol{\omega}_m(\sigma) - \alpha\mathbf{a}_m(\sigma)d\sigma\right]\right)\mathbf{a}_m(t_1)\neq 0. \tag{18}$$

PROOF. The transition matrix associated with matrix $\mathbf{A}(t)$ is given by (19), where $\mathbf{R}_{\boldsymbol{\psi}}(t)\in SO(3)$ is such that

$$\dot{\mathbf{R}}_{\boldsymbol{\psi}}(t) = \mathbf{R}_{\boldsymbol{\psi}}(t)\mathbf{S}\left[\boldsymbol{\omega}_m(t) - \alpha\mathbf{a}_m(t)\right], \quad \mathbf{R}_{\boldsymbol{\psi}}(t_0) = \mathbf{I}. \tag{20}$$

Since, by construction, $\boldsymbol{\phi}(t_0,t_0) = \mathbf{I}$, it is straightforward to verify (19) by recalling the transition matrix property $\frac{\partial\boldsymbol{\phi}(t,t_0)}{\partial t} = \mathbf{A}(t)\boldsymbol{\phi}(t,t_0)$. The observability of the LTV system (15) is characterized by the observability Gramian associated with the pair $(\mathbf{A}(t),\mathbf{C}(t))$, which can be expressed as

$$\boldsymbol{\mathcal{W}}(t_0,t) = \int_{t_0}^{t}\boldsymbol{\phi}^\mathsf{T}(\tau,t_0)\mathbf{C}^\mathsf{T}(\tau)\mathbf{C}(\tau)\boldsymbol{\phi}(\tau,t_0)d\tau \quad \in\mathbb{R}^{12\times 12}. \tag{21}$$

Consider now a constant unit vector $\mathbf{d} = \left[\mathbf{d}_1^\mathsf{T}, \mathbf{d}_2^\mathsf{T}, \mathbf{d}_3^\mathsf{T}, \mathbf{d}_4^\mathsf{T}\right]^\mathsf{T}\in\mathbb{R}^{12}$, with $\mathbf{d}_1$,$\mathbf{d}_2$,$\mathbf{d}_3$,$\mathbf{d}_4 \in\mathbb{R}^3$, and further notice that $\mathbf{d}^\mathsf{T}\boldsymbol{\mathcal{W}}(t_0,t)\mathbf{d} = \int_{t_0}^{t}\|\mathbf{f}(\tau,t_0)\|^2 d\tau$, where $\mathbf{f}(\tau,t_0) = \begin{bmatrix}\mathbf{f}_1(\tau,t_0)\\ f_2(\tau,t_0)\end{bmatrix}\in\mathbb{R}^4$, with $\mathbf{f}_1(\tau,t_0) := \mathbf{d}_1 - \int_{t_0}^{\tau}\mathbf{S}\left[\mathbf{a}_m(\sigma)\right]\mathbf{R}_{\boldsymbol{\psi}}^\mathsf{T}(\sigma)d\sigma\mathbf{d}_2 + \left(\int_{t_0}^{\tau}\mathbf{S}\left[\boldsymbol{\omega}_m(\sigma)\right]d\sigma + \mathbf{I}\right)\mathbf{d}_3 - \int_{t_0}^{\tau}\mathbf{S}\left[\mathbf{a}_m(\sigma)\right]d\sigma\mathbf{d}_4\in\mathbb{R}^3$, and

$$f_2(\tau,t_0) := \mathbf{d}_2^\mathsf{T}\mathbf{R}_{\boldsymbol{\psi}}(\tau)\mathbf{a}_m(\tau)\in\mathbb{R}. \tag{22}$$

By computing the first two derivatives of $\mathbf{f}(\tau,t_0)$ with respect to τ, we conclude that both are norm-bounded from above on $\mathcal{T}$ as all quantities involved are norm bounded as well.

To show that (17) is necessary, start by supposing that it is not verified, which means $\forall_{\substack{t_1\in\mathcal{T}\\ c_1,c_2\in\mathbb{R}\setminus\{0\}}} \; c_1\mathbf{a}_m(t_0)\times\mathbf{a}_m(t_1) + c_2\boldsymbol{\omega}_m(t_0)\times\boldsymbol{\omega}_m(t_1) = \mathbf{0}$. Then, let $\mathbf{d}_2 = \mathbf{0}$, $\mathbf{d}_1 = -\mathbf{d}_3 \neq \mathbf{0}$, with $\mathbf{d}_3 = c_2\boldsymbol{\omega}_m(t_0)$, and $\mathbf{d}_4 = -c_1\mathbf{a}_m(t_0)$, for some $c_1,c_2\in\mathbb{R}\setminus\{0\}$, such that $\|\mathbf{d}\| = 1$. As result, it follows that $\mathbf{f}(\tau,t_0) = \mathbf{0}$. Note that if $\boldsymbol{\omega}_m(t_0) = \mathbf{0}$, in which case it must be $c_1 = 1/\|\mathbf{a}_m(t_0)\|$, the last result still holds. This allows us to conclude that the observability Gramian (21) is singular, therefore the LTV system (15) is not observable. By contraposition, if the LTV system (15) is observable, then the observabilty condition (17) must be true.

To show that both observability conditions (17) and (18) are sufficient, notice first that, for some $\tau\in\mathcal{T}$, if $f_2(\tau,t_0)\neq 0$, then it follows, using [22, *Proposition* 4.2], that $\mathbf{d}^\mathsf{T}\boldsymbol{\mathcal{W}}(t_0,t)\mathbf{d} > 0$. Likewise, for some $\tau\in\mathcal{T}$, if $\frac{d}{d\tau}f_2(\tau,t_0)\neq 0$, then it follows, using [22, *Proposition* 4.2] twice, that $\mathbf{d}^\mathsf{T}\boldsymbol{\mathcal{W}}(t_0,t)\mathbf{d} > 0$. Otherwise, according to (22), if $f_2(\tau,t_0) = 0$ for all $\tau\in\mathcal{T}$, this means that either the vector $\mathbf{R}_{\boldsymbol{\psi}}(\tau)\mathbf{a}_m(\tau)$ is always orthogonal to $\mathbf{d}_2$, or $\mathbf{d}_2 = \mathbf{0}$. In particular, since $\mathbf{R}_{\boldsymbol{\psi}}(t_0) = \mathbf{I}$, one has $\mathbf{d}_2\perp\mathbf{a}_m(t_0)$. Since the solution of (20) is given by

$$\mathbf{R}_{\boldsymbol{\psi}}(t) = \exp\left(\mathbf{S}\left[\int_{t_0}^{t}\boldsymbol{\omega}_m(\sigma) - \alpha\mathbf{a}_m(\sigma)d\sigma\right]\right), \; t\geq t_0, \tag{23}$$

substituting (23) in (22) allows us to conclude that it must be

$$\mathbf{d}_2^\mathsf{T}\exp\left(\mathbf{S}\left[\int_{t_0}^{\tau}\boldsymbol{\omega}_m(\sigma) - \alpha\mathbf{a}_m(\sigma)d\sigma\right]\right)\mathbf{a}_m(\tau) = 0 \tag{24}$$

for all $\tau\in\mathcal{T}$. But, according to (18), there exists an instant $\tau = t_1$ when, given $\mathbf{v} = \mathbf{d}_2$, the zero identity in (24) cannot hold. Hence, for $f_2(\tau,t_0) = 0$ to hold for all $\tau\in\mathcal{T}$ it must be $\mathbf{d}_2 = \mathbf{0}$. Evaluate now $\|\mathbf{f}(\tau,t_0)\|$ at $\tau = t_0$, which results in

$$\|\mathbf{f}(t_0,t_0)\| = \left\|\begin{bmatrix}\mathbf{d}_1 + \mathbf{d}_3\\ 0\end{bmatrix}\right\|, \tag{25}$$

and suppose that $\mathbf{d}_3\neq\mathbf{0}$. Then, if $\mathbf{d}_1\neq -\mathbf{d}_3$, it follows from (25) that $\|\mathbf{f}(t_0,t_0)\| > 0$ and, from [22, *Proposition* 4.2], it must be $\mathbf{d}^\mathsf{T}\boldsymbol{\mathcal{W}}(t_0,t)\mathbf{d} > 0$. Consider the case when $\mathbf{d}_1 = -\mathbf{d}_3$, with $\mathbf{d}_3\neq\mathbf{0}$ and $\mathbf{d}_4\neq\mathbf{0}$ as well. In this case, $\|\mathbf{f}(t_0,t_0)\| = 0$ and $\frac{d}{d\tau}\mathbf{f}(\tau,t_0) = \begin{bmatrix}\mathbf{S}\left[\mathbf{a}_m(\tau)\right]\mathbf{d}_4 - \mathbf{S}\left[\boldsymbol{\omega}_m(\tau)\right]\mathbf{d}_3\\ \mathbf{0}\end{bmatrix}$. If $\frac{d}{d\tau}\mathbf{f}(\tau,t_0)\neq\mathbf{0}$, then, using [22, *Proposition* 4.2] twice, it follows that $\mathbf{d}^\mathsf{T}\boldsymbol{\mathcal{W}}(t_0,t)\mathbf{d} > 0$. Otherwise, if $\frac{d}{d\tau}\mathbf{f}(\tau,t_0) = \mathbf{0}$, then the following must hold:

$$\mathbf{S}\left[\mathbf{a}_m(\tau)\right]\mathbf{d}_4 - \mathbf{S}\left[\boldsymbol{\omega}_m(\tau)\right]\mathbf{d}_3 = \mathbf{0}. \tag{26}$$

The identity in (26) establishes that the four vector entities, $\mathbf{a}_m(\tau)$, $\mathbf{d}_4$, $\boldsymbol{\omega}_m(\tau)$ and $\mathbf{d}_3$, must be coplanar for all $\tau\in\mathcal{T}$. However, according to the first observability condition (17), that geometric relationship cannot be verified for all $\tau\in\mathcal{T}$, which means it must be simultaneously $\mathbf{d}_3 = \mathbf{d}_4 = \mathbf{0}$ in order for (26) to hold. But, since $\mathbf{d}_1 = -\mathbf{d}_3$, this would in turn imply that $\mathbf{d} = \mathbf{0}$, which contradicts the claim that $\mathbf{d}$ is a unit vector. Therefore, it has been shown that $\mathbf{d}^\mathsf{T}\boldsymbol{\mathcal{W}}(t_0,t)\mathbf{d} > 0$ for all $\|\mathbf{d}\| = 1$, which means the observability Gramian (21) is always positive definite and thus the LTV system (15) is observable. This concludes the proof. ■

It has just been shown that the LTV system (15) is observable, but stronger forms of observability, in particular uniform complete observability, can be attained by considering persistency of excitation conditions, for instance, by conveniently applying uniform bounds to both (17) and (18). Afterwards, by following similar steps as those presented in the proof of *Theorem* 3, it is possible to conclude that the LTV system (15) is also uniformly completely observable, therefore ensuring that, in nominal terms, the KF (16) offers globally exponentially stable guarantees.

$$\boldsymbol{\phi}(t,t_0) = \begin{bmatrix} \mathbf{I} & -\int_{t_0}^{t} \mathbf{S}\left[\mathbf{a}_m(\sigma)\right] \mathbf{R}_{\boldsymbol{\psi}}^{\mathsf{T}}(\sigma) d\sigma & \int_{t_0}^{t} \mathbf{S}\left[\boldsymbol{\omega}_m(\sigma)\right] d\sigma & -\int_{t_0}^{t} \mathbf{S}\left[\mathbf{a}_m(\sigma)\right] d\sigma \\ \mathbf{0} & \mathbf{R}_{\boldsymbol{\psi}}^{\mathsf{T}}(t) & \mathbf{0} & \mathbf{0} \\ \mathbf{0} & \mathbf{0} & \mathbf{I} & \mathbf{0} \\ \mathbf{0} & \mathbf{0} & \mathbf{0} & \mathbf{I} \end{bmatrix} \in \mathbb{R}^{12\times 12} \tag{19}$$

3 Rotation Matrix Estimation

Consider the following observer for the rotation matrix:

$$\begin{aligned} \dot{\hat{\mathbf{R}}}(t) = \hat{\mathbf{R}}(t)\mathbf{S}\Big[&\boldsymbol{\omega}_m(t) - \hat{\mathbf{b}}_{\boldsymbol{\omega}} - \hat{\mathbf{R}}^{\mathsf{T}}(t)\,{}^{I}\boldsymbol{\omega}_E + \\ &+ k_{\boldsymbol{\omega}_E}\mathbf{S}\left[\hat{\boldsymbol{\omega}}_E(t)\right]\hat{\mathbf{R}}^{\mathsf{T}}(t)\,{}^{I}\boldsymbol{\omega}_E + k_{\mathbf{g}}\mathbf{S}\left[\hat{\mathbf{g}}(t)\right]\hat{\mathbf{R}}^{\mathsf{T}}(t)\,{}^{I}\mathbf{g}\Big], \end{aligned} \tag{27}$$

where $k_{\boldsymbol{\omega}_E}$ and $k_{\mathbf{g}}$ are positive tuning constants, and where $\hat{\mathbf{R}}(t) \in SO(3)$ denotes the estimates of $\mathbf{R}(t)$. This observer completes the cascade structure of the proposed attitude estimation solution, which is illustrated in Figure 1.

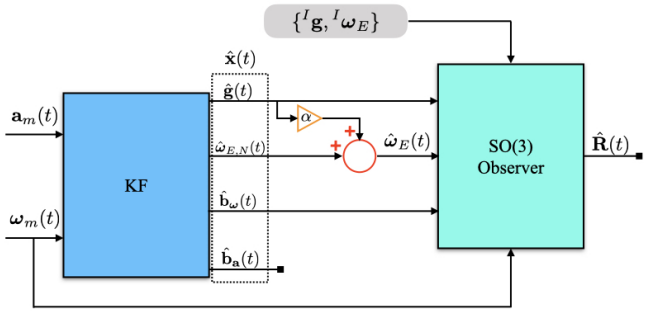

Figure 1. Implementation scheme of the attitude estimation cascade.

Define the error variables

$$\tilde{\mathbf{R}}(t) := \mathbf{R}(t)\hat{\mathbf{R}}^{\mathsf{T}}(t) \in SO(3), \tag{28}$$

$\tilde{\mathbf{b}}_{\boldsymbol{\omega}}(t) := \mathbf{b}_{\boldsymbol{\omega}} - \hat{\mathbf{b}}_{\boldsymbol{\omega}}(t)$, $\tilde{\boldsymbol{\omega}}_E(t) := \boldsymbol{\omega}_E(t) - \hat{\boldsymbol{\omega}}_E(t)$ and, finally, $\tilde{\mathbf{g}}(t) := \mathbf{g}(t) - \hat{\mathbf{g}}(t)$. The derivative of (28) follows as $\dot{\tilde{\mathbf{R}}}(t) = \dot{\mathbf{R}}(t)\hat{\mathbf{R}}^{\mathsf{T}}(t) + \mathbf{R}(t)\dot{\hat{\mathbf{R}}}^{\mathsf{T}}(t)$, which, by using equations (1) and (2), the nonlinear observer (27), and the error variables formerly defined, results, after a few straightforward computations, in

$$\begin{aligned} \dot{\tilde{\mathbf{R}}}(t) = \boldsymbol{\eta}(t, \tilde{\mathbf{b}}_{\boldsymbol{\omega}}, \tilde{\boldsymbol{\omega}}_E, \tilde{\mathbf{g}}) - \mathbf{S}\left[(\mathbf{I} - \tilde{\mathbf{R}}(t))\,{}^{I}\boldsymbol{\omega}_E\right]\tilde{\mathbf{R}}(t) + \\ - k_{\boldsymbol{\omega}_E}\mathbf{S}\Big[\mathbf{S}\left[{}^{I}\boldsymbol{\omega}_E\right]\tilde{\mathbf{R}}(t)\,{}^{I}\boldsymbol{\omega}_E\Big]\tilde{\mathbf{R}}(t) - k_{\mathbf{g}}\mathbf{S}\Big[\mathbf{S}\left[{}^{I}\mathbf{g}\right]\tilde{\mathbf{R}}(t)\,{}^{I}\mathbf{g}\Big]\tilde{\mathbf{R}}(t), \end{aligned} \tag{29}$$

with the *perturbation* function $\boldsymbol{\eta}(\cdot)$ given by

$$\begin{aligned} \boldsymbol{\eta}(t, \tilde{\mathbf{b}}_{\boldsymbol{\omega}}, \tilde{\boldsymbol{\omega}}_E, \tilde{\mathbf{g}}) = &-\mathbf{S}\left[\mathbf{R}(t)\tilde{\mathbf{b}}_{\boldsymbol{\omega}}(t)\right]\tilde{\mathbf{R}}(t) + \\ &+ k_{\boldsymbol{\omega}_E}\mathbf{S}\left[\mathbf{S}\left[\mathbf{R}(t)\tilde{\boldsymbol{\omega}}_E(t)\right]\tilde{\mathbf{R}}(t)\,{}^{I}\boldsymbol{\omega}_E\right]\tilde{\mathbf{R}}(t) + \\ &+ k_{\mathbf{g}}\mathbf{S}\left[\mathbf{S}\left[\mathbf{R}(t)\tilde{\mathbf{g}}(t)\right]\tilde{\mathbf{R}}(t)\,{}^{I}\mathbf{g}\right]\tilde{\mathbf{R}}(t). \end{aligned} \tag{30}$$

Next, define the domain $D := [0,\, \pi]$, and consider the Euler angle-axis representation of the error associated with $\tilde{\mathbf{R}}$,

$$\tilde{\mathbf{R}}(\tilde{\theta},\tilde{\mathbf{v}}) = \mathbf{I} + \sin(\tilde{\theta}(t))\mathbf{S}[\tilde{\mathbf{v}}(t)] + \Big[1 - \cos(\tilde{\theta}(t))\Big]\,\mathbf{S}^2\left[\tilde{\mathbf{v}}(t)\right], \tag{31}$$

where $\tilde{\theta}(t) \in D$ and $\tilde{\mathbf{v}}(t) \in S(2)$ form the Euler angle-axis pair, also known as the exponential coordinates of $\tilde{\mathbf{R}}$. In the sequel, consider as well the square of (31), which also consists in a rotation matrix, and is given by

$$\tilde{\mathbf{R}}^2(\tilde{\theta},\tilde{\mathbf{v}}) = \mathbf{I} + \sin(2\tilde{\theta}(t))\mathbf{S}\left[\tilde{\mathbf{v}}(t)\right] + 2\sin^2(\tilde{\theta}(t))\mathbf{S}^2[\tilde{\mathbf{v}}(t)]. \tag{32}$$

The following theorem is the main result of this paper.

Theorem 4 *Consider the attitude observer* (27)*, the error definition* (28)*, the FOG readings of angular velocity* (2)*, the acceleration measurements* (3)*, and the estimates of the KF* (16)*. Suppose* Assumptions *1 and 2 are verified, and define the set* $\Omega \subset SO(3)$ *as* $\Omega := \{\tilde{\mathbf{R}}(t),\, \boldsymbol{\eta}(t,\, \tilde{\mathbf{b}}_{\boldsymbol{\omega}},\, \tilde{\boldsymbol{\omega}}_E,\, \tilde{\mathbf{g}}) = \mathbf{0} \mid \mathrm{tr}(\tilde{\mathbf{R}}(t)) = -1\}$*. In view of* $\tilde{\mathbf{R}}(t)$ *expressed in terms of the unit quaternion, cf.* (A.1) *in Appendix, define as well the parameterized set* $\Theta(\zeta) := \{\tilde{\mathbf{R}}(\tilde{s},\, \tilde{\mathbf{r}}) \in SO(3) : \tilde{s} \geq \zeta\}$*. Then: i) the set* Ω *is forward invariant and unstable with respect to the observer dynamics* (27)*; ii) when considering* $\boldsymbol{\eta}(t,\, \tilde{\mathbf{b}}_{\boldsymbol{\omega}},\, \tilde{\boldsymbol{\omega}}_E,\, \tilde{\mathbf{g}}) \equiv \mathbf{0}$*, the rotation matrix error* $\tilde{\mathbf{R}}(t)$ *converges locally exponentially fast to* $\mathbf{I}$*, and is AGAS to* $\mathbf{I}$*; and, iii) fixing* $0 < \zeta < 1$*, the nonlinear error dynamics* (29) *are LISS with* (30) *as input, and, for all initial conditions such that* $\tilde{\mathbf{R}}(t_0) \in \Theta(\zeta)$*,* $\tilde{\mathbf{R}}(t) \to \mathbf{I}$*, i.e.,* $\hat{\mathbf{R}}(t) \to \mathbf{R}(t)$*.*

PROOF. Let $V : D \to \mathbb{R}$ be a positive bounded Lyapunov-like candidate function given by $V(\tilde{\theta}) := 1 - \cos(\tilde{\theta}(t)) = \frac{1}{2}\mathrm{tr}(\mathbf{I} - \tilde{\mathbf{R}}(t))$. The time derivative of V satisfies $\dot{V}(t) = -\frac{1}{2}\mathrm{tr}(\dot{\tilde{\mathbf{R}}}(t))$. Start by considering the *unforced* dynamics, i.e., the case when $\boldsymbol{\eta} \equiv \mathbf{0}$ holds. Then, by noticing that $\mathrm{tr}(\mathbf{S}[(\mathbf{I} - \tilde{\mathbf{R}}(t))\,{}^{I}\boldsymbol{\omega}_E]\tilde{\mathbf{R}}(t)) = 0$, equation $\dot{V}(t)$ can be written as

$$\begin{aligned} \dot{V}(t) = &\frac{k_{\boldsymbol{\omega}_E}}{2}\,\mathrm{tr}\Big(\mathbf{S}\Big[\mathbf{S}\left[{}^{I}\boldsymbol{\omega}_E\right]\tilde{\mathbf{R}}(t)\,{}^{I}\boldsymbol{\omega}_E\Big]\tilde{\mathbf{R}}(t)\Big) + \\ &+ \frac{k_{\mathbf{g}}}{2}\,\mathrm{tr}\Big(\mathbf{S}\Big[\mathbf{S}\left[{}^{I}\mathbf{g}\right]\tilde{\mathbf{R}}(t)\,{}^{I}\mathbf{g}\Big]\tilde{\mathbf{R}}(t)\Big). \end{aligned} \tag{33}$$

The property $\mathbf{S}\left[\mathbf{S}\left[\mathbf{a}\right]\mathbf{b}\right] = \mathbf{b}\mathbf{a}^{\mathsf{T}} - \mathbf{a}\mathbf{b}^{\mathsf{T}}$ helps rewriting (33) as $\dot{V}(t) = -\frac{k_{\boldsymbol{\omega}_E}}{2}\|{}^{I}\boldsymbol{\omega}_E\|^2 + \frac{k_{\boldsymbol{\omega}_E}}{2}\,\mathrm{tr}(\tilde{\mathbf{R}}^2(t)\,{}^{I}\boldsymbol{\omega}_E\,{}^{I}\boldsymbol{\omega}_E^{\mathsf{T}}) - \frac{k_{\mathbf{g}}}{2}\|{}^{I}\mathbf{g}\|^2 + \frac{k_{\mathbf{g}}}{2}\,\mathrm{tr}(\tilde{\mathbf{R}}^2(t)\,{}^{I}\mathbf{g}\,{}^{I}\mathbf{g}^{\mathsf{T}})$. Replacing (32) in the previous expression yields $\dot{V}(t) = -\sin^2(\tilde{\theta}(t))(k_{\boldsymbol{\omega}_E}\left\|{}^{I}\boldsymbol{\omega}_E \times \tilde{\mathbf{v}}(t)\right\|^2 + k_{\mathbf{g}}\left\|{}^{I}\mathbf{g} \times \tilde{\mathbf{v}}(t)\right\|^2) \leq 0$. Under *Assumption* 1, $\tilde{\mathbf{v}}(t)$ cannot be simultaneously collinear with both ${}^{I}\boldsymbol{\omega}_E$ and ${}^{I}\mathbf{g}$, which means $\dot{V}(t) = 0$ is satisfied only on two occasions, when: 1) $\tilde{\theta}(t) = \pi$, which, according to (31), corresponds to the condition $\mathrm{tr}(\tilde{\mathbf{R}}(t)) = -1$, with $\tilde{\mathbf{R}}(t) = \tilde{\mathbf{R}}^{\mathsf{T}}(t)$; and, 2) $\tilde{\theta}(t) = 0$, which means $\tilde{\mathbf{R}}(t) = \mathbf{I}$. With $\tilde{\theta}(t) = \pi$, the derivative of $\mathrm{tr}(\tilde{\mathbf{R}}(t))$ is zero, which asserts forward invariance of Ω. Accordingly, by applying LaSalle's principle to the solutions of (29), one concludes that $\tilde{\mathbf{R}}(t)$ converges asymptotically to either $\mathbf{I}$ or some rotation matrix belonging to Ω. In *Lemma* 5, in Appendix, local exponential stability of the isolated equilibrium point $\mathbf{I}$ is shown through the linearization of the quaternion dynamics associated with the *unforced* error dynamics, i.e., when $\boldsymbol{\eta} \equiv \mathbf{0}$ holds, thus proving the theorem's statement ii).

Resorting again to the quaternion formulation, the forward invariant set Ω associated with the case when $\boldsymbol{\eta} \equiv \mathbf{0}$ holds

is described by $\Omega = \left\{(\tilde{s}, \tilde{\mathbf{r}}) \mid \tilde{s} = 0, \tilde{\mathbf{r}}^{\mathsf{T}}\tilde{\mathbf{r}} = 1\right\}$. Then, from (A.4), and in view of *Assumption* 1, it follows that the dynamics of $\tilde{s}(t)$ are unstable for any point $\tilde{s} \neq 0$. Therefore, $\tilde{s}(t)$ is a strictly increasing function for all $t \geq 0$, which means the set Ω corresponds to an unstable equilibrium point. This proves the theorem's statement i). The third and last statement of the theorem is proved considering the Lyapunov-like function $V(\tilde{\mathbf{r}}) := 1/2\|\tilde{\mathbf{r}}(t)\|^2$. From (A.3), the derivative of this function is given by $\dot{V}(\tilde{\mathbf{r}},t) = -\gamma(\tilde{\mathbf{r}})\left(1 - \|\tilde{\mathbf{r}}(t)\|^2\right) + \frac{\tilde{s}(t)}{2}\tilde{\mathbf{r}}^{\mathsf{T}}(t)\tilde{\boldsymbol{\omega}}_{\boldsymbol{\eta}}(t)$. Since $\gamma(\tilde{\mathbf{r}}) \geq \epsilon\|\tilde{\mathbf{r}}(t)\|^2$ (cf. [23, *Lemma* 11]), where $\epsilon = \frac{k_{\boldsymbol{\omega}_E} k_{\mathbf{g}}}{k_{\boldsymbol{\omega}_E}\|{}^I\boldsymbol{\omega}_E\|^2 + k_{\mathbf{g}}\|{}^I\mathbf{g}\|^2}\left\|{}^I\boldsymbol{\omega}_E \times {}^I\mathbf{g}\right\|^2 > 0$, and since, by definition, $\tilde{s}^2(t) = 1 - \|\tilde{\mathbf{r}}(t)\|^2$ and $\tilde{s}(t) \leq 1$, it follows that $\dot{V}(\tilde{\mathbf{r}},t) \leq -\epsilon\|\tilde{\mathbf{r}}(t)\|\left(\|\tilde{\mathbf{r}}(t)\|\tilde{s}^2(t) - \frac{1}{2\epsilon}\|\tilde{\boldsymbol{\omega}}_{\boldsymbol{\eta}}(t)\|\right)$. Now, fix $0 < \theta < 1$, such that $\dot{V}(\tilde{\mathbf{r}},t) \leq -\epsilon(1-\theta)\|\tilde{\mathbf{r}}(t)\|^2\tilde{s}^2(t) - \|\tilde{\mathbf{r}}(t)\|\left(\theta\epsilon\|\tilde{\mathbf{r}}(t)\|\tilde{s}^2(t) - \frac{1}{2}\|\tilde{\boldsymbol{\omega}}_{\boldsymbol{\eta}}(t)\|\right)$. This allows us to conclude that $\dot{V}(\tilde{\mathbf{r}},t) \leq -\epsilon(1-\theta)\|\tilde{\mathbf{r}}(t)\|^2\tilde{s}^2(t)\ \forall\ \|\tilde{\mathbf{r}}(t)\| \geq \beta\|\tilde{\boldsymbol{\omega}}_{\boldsymbol{\eta}}(t)\|$, with constant β fixed as $\beta := 1/(2\epsilon\theta\zeta^2)$. As result of $\dot{V}(\tilde{\mathbf{r}},t) \leq 0$ for all $\|\tilde{\mathbf{r}}(t)\| \geq \beta\|\tilde{\boldsymbol{\omega}}_{\boldsymbol{\eta}}(t)\|$, $V(t)$ is non-increasing for all $\|\tilde{\mathbf{r}}(t)\| \geq \beta\|\tilde{\boldsymbol{\omega}}_{\boldsymbol{\eta}}(t)\|$, which means $\tilde{s}(t)$ is non-decreasing for all $\|\tilde{\mathbf{r}}(t)\| \geq \beta\|\tilde{\boldsymbol{\omega}}_{\boldsymbol{\eta}}(t)\|$. Therefore, for all initial conditions $\tilde{\mathbf{R}}(t_0) \in \Theta(\zeta)$ and $\|\tilde{\mathbf{r}}(t)\| \geq \beta\|\tilde{\boldsymbol{\omega}}_{\boldsymbol{\eta}}(t)\|$, it follows that $\tilde{s}(t) \geq \zeta$ for all $t \geq t_0$, which implies $\dot{V}(\tilde{\mathbf{r}},t) \leq -\epsilon(1-\theta)\|\tilde{\mathbf{r}}(t)\|^2\zeta^2$ for all $\|\tilde{\mathbf{r}}(t)\| \geq \beta\|\tilde{\boldsymbol{\omega}}_{\boldsymbol{\eta}}(t)\|$ and $\tilde{\mathbf{R}}(t_0) \in \Theta(\zeta)$. Then, invoking [24, *Theorem* 5.2] proves, finally, that the dynamics $\dot{\tilde{\mathbf{r}}}(t)$ are LISS with (30) as input. It follows that $\tilde{\mathbf{r}}(t) \to \mathbf{0}$, or, equivalently, $\tilde{\mathbf{R}}(t) \to \mathbf{I}$, thus concluding the proof. ■

4 Experimental Results

In order to validate the cascade attitude estimation solution, an experiment was carried out using a tri-axial high-grade FOG Inertial Measurement Unit (IMU) KVH 1775 mounted on a Ideal Aerosmith Model 2103HT Three-Axis Positioning and Motion Rate Table (MRT), which is designed to provide precise position, rate, and acceleration motion, for instance, for the development and/or production testing and calibration of IMUs and inertial navigation systems. The final experimental setup, located at a latitude of $\varphi = 38.777816$ (deg), a longitude of $\psi = 9.097570$ (deg), and at sea level, is depicted in Figure 2.

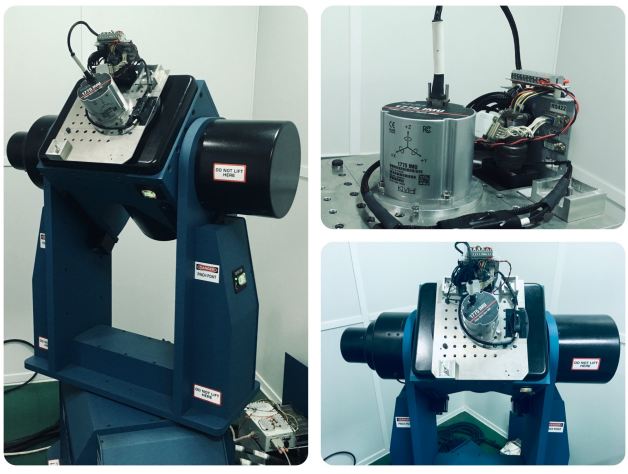

Figure 2. Experimental setup for attitude estimation.

The KVH 1775 provides tri-axial readings of angular velocity and acceleration. Slow rotational maneuvers are considered to ensure that the magnitude of the gravitational field is the dominant acceleration term, i.e., to guarantee that the approximation (4) is valid. At room temperature, this unit's accelerometer is characterized by a velocity random walk of 0.12 (mg/$\sqrt{\text{Hz}}$), as mentioned in the previous section.

Based on previous work by the authors [25], a calibration procedure was implemented beforehand to determine, for both the high grade rate gyro and accelerometer included in the KVH 1775, a matrix of constant scaling factors, a constant bias and a corresponding inertial vector (with respect to the MRT's own local NED inertial frame). The inertial reference vectors, as result of the calibration routine, were ${}^I\boldsymbol{\omega}_E = [-0.9060\ \ -11.7102\ \ -9.3959]^{\mathsf{T}}$ (deg/h) and ${}^I\mathbf{g} = [0.0170\ \ -0.0049\ \ 9.8006]^{\mathsf{T}}$ (m/s^2). In regard to the sensor biases, $\mathbf{b}_{\mathbf{a}}$ and $\mathbf{b}_{\boldsymbol{\omega}}$, it was observed during the full calibration of the KVH 1775 that these changed between tests. However, the extensive results presented in [25] still allow for a reliable qualitative prediction, which shall be used only as reference for performance, in particular of the KF (16). More specifically, the bias calibration data in [25] suggests that $\mathbf{b}_{\mathbf{a}}$ has x and y components around zero and a strong z component around 0.9 (mg). In turn, $\mathbf{b}_{\boldsymbol{\omega}}$ has a strong negative x component around -0.7 (deg/h) while its components y and z are close to each other and display a mirrored behavior. Naturally, to properly assess the performance of the cascade methodology, the sensor measurements $\boldsymbol{\omega}_m(t)$ and $\mathbf{a}_m(t)$, as given by (2) and (3), respectively, were not bias corrected.

Data acquired from the MRT were sampled at 128 (Hz), and later appropriately down-sampled to 25 (Hz) to match the sampling frequency of the KVH 1775.

The MRT was programmed to describe a three-dimensional rotational maneuver lasting approximately one hour.

The KF (16) was tuned as follows: the initial state estimate was set to $\hat{\mathbf{x}}(t_0) = [\mathbf{a}_m^{\mathsf{T}}(t_0),\ \mathbf{0},\ \mathbf{0},\ \mathbf{0}]^{\mathsf{T}}$; the initial state error covariance matrix was set to $\mathbf{P}(t_0) = \text{diag}(10^{-2}\mathbf{I},\ 10^{-6}\mathbf{I},\ 10^{-3}\mathbf{I},\ 10^{-6}\mathbf{I})$; and, finally, the covariance matrices of the process and observation noises were set to $\boldsymbol{\mathcal{Q}} = \text{diag}(10^{-6}\mathbf{I},\ 10^{-13}\mathbf{I},\ 10^{-16}\mathbf{I},\ 10^{-16}\mathbf{I})$ and $\boldsymbol{\mathcal{R}} = \text{diag}(10^{-7}\mathbf{I},\ 10^{-7})$, respectively. These values were all adjusted empirically for the best performance. In the experiments, the rotation matrix observers gains were also set in a piece-wise fashion, as described in Table 1.

Table 1
Observer gains used in the experiments.

time (min)	$k_{\boldsymbol{\omega}_E}\|{}^I\boldsymbol{\omega}_E\|^2$	$k_{\mathbf{g}}\|{}^I\mathbf{g}\|^2$
$t < 7.5$	0.02	20
$7.5 \leq t < 15$	0.005	15
$15 \leq t < 22.5$	0.001	5
$22.5 \leq t < 30$	7.5×10^{-4}	2.5
$30 \leq t < 50$	1×10^{-4}	2.5
$t \geq 50$	1×10^{-5}	1

The experimental estimation error of $\boldsymbol{\omega}_{E,N}(t)$ remains most of the time below 1 (deg/h), with a steady-state accuracy around 0.4 (deg/h), as indicated in Table 1. This strongly hints at an efficient and highly accurate performance of the KF (16) in real world applications.

The evolutions of $\hat{\mathbf{b}}_{\mathbf{a}}(t)$ and $\hat{\mathbf{b}}_{\boldsymbol{\omega}}(t)$ are shown in Figures 4 and 5, respectively. Both plots suggest that the biases, despite having been assumed constant, change slightly over time, which is in line with expectations and further demonstrates that the proposed KF is capable of tracking slow variations. This notwithstanding, the results resemble the qualitative prediction stated before. Indeed, the z component of $\hat{\mathbf{b}}_{\mathbf{a}}(t)$ converges to 0.75 (mg), whereas the other two components have

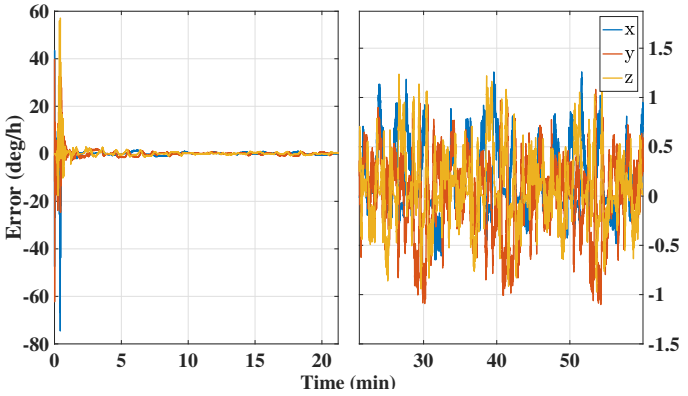

Figure 3. Estimation error of $\boldsymbol{\omega}_{E,N}(t)$.

smaller magnitude. The KVH 1775's manufacturer specifies a maximum bias offset of ± 0.5 (mg), which means that the overshoot could be not only due to the accelerometers performance but also due to the accuracy of the MRT. Regarding the evolution of $\hat{\mathbf{b}}_{\boldsymbol{\omega}}(t)$, its y and z components are close to each other and display a mirrored behavior, while the x component evolves towards a negative value of -1.5 (deg/h). The absence of ground-truth bias information in the experiments certainly prevents a more rigorous analysis, but, overall, the KF (16) seems to provide a coherent estimation of both sensor biases. What's more, the next results, which concern the estimation of the rotation matrix, shall further attest to its goodness.

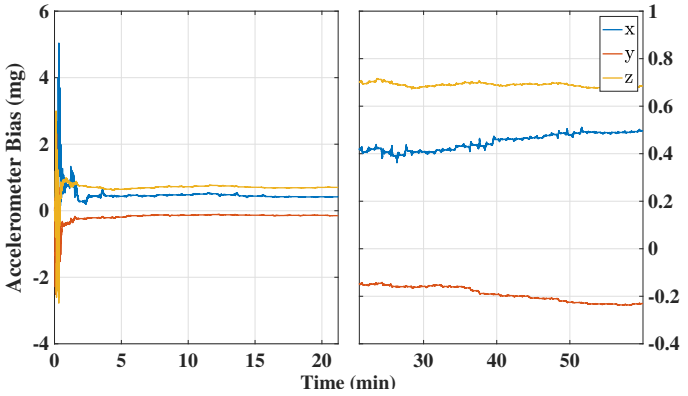

Figure 4. Evolution of $\hat{\mathbf{b}}_{\mathbf{a}}(t)$.

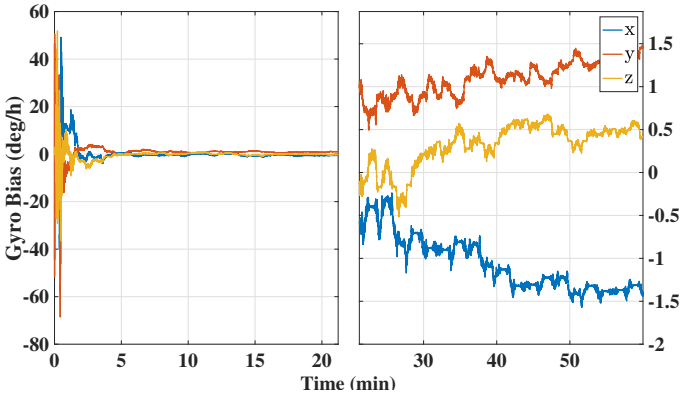

Figure 5. Evolution of $\hat{\mathbf{b}}_{\boldsymbol{\omega}}(t)$.

The initial rotation matrix estimate was such that its corresponding angle deviation was approximately 128 (deg).

The evolution of the angle error, which reaches steady-state around the same time, approaches a neighborhood of zero, as shown in Figure 6. Notice also the quick initial convergence, which allows for the correction of large angle deviations in under a few minutes. Furthermore, the mean angle deviation, computed for 45 (min) $\leq t \leq$ 60 (min), was 0.40751 (deg), as documented in Table 2. Once again, this demonstrates the high level of accuracy that the proposed solution can attain.

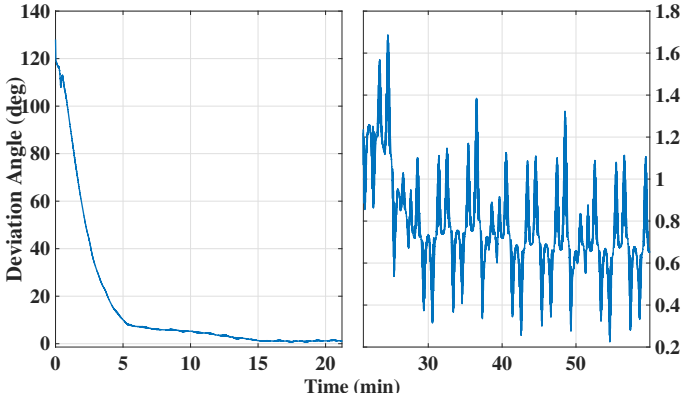

Figure 6. Time evolution of $\tilde{\theta}(t)$ for $\tilde{\theta}(0) = 128$ (deg).

Table 2
Experimental steady-state statistics for 45 min $\leq t \leq$ 60 min

variable	mean	sd.	units
$\mathbf{g}(t) - \hat{\mathbf{g}}(t)$	0.0011167	1.7507	mg
$\boldsymbol{\omega}_{E,N}(t) - \hat{\boldsymbol{\omega}}_{E,N}(t)$	0.055817	0.39762	deg/h
$\|\hat{\mathbf{b}}_{\mathbf{a}}(t)\|$	0.86663	0.0076772	mg
$\|\hat{\mathbf{b}}_{\boldsymbol{\omega}}(t)\|$	1.8711	0.1065	deg/h
$\|\hat{\boldsymbol{\omega}}_{E}(t)\|$	14.922	0.34267	deg/h
$\tilde{\theta}(t)$	0.40751	0.16467	deg

5 Conclusions

This paper presented a cascade solution for the problem of attitude and bias estimation. The first part of the cascade consists in a KF applied to an LTV system whose state comprises: the vector of gravitational acceleration; two constant sensor bias offsets; and, the component of the Earth's angular velocity that spans the North and East directions of the local inertial NED frame. The LTV system was shown to be uniformly observable, which in turn guarantees global exponential stability of the error dynamics associated with the KF estimates. The second part of the cascade features a nonlinear attitude observer, built on $SO(3)$, that is driven by measurements of angular velocity provided by a set of high-grade FOGs, in addition to the estimates of the KF. By regarding the rotation error dynamics as a perturbed system with vanishing perturbation, the nonlinear attitude observer was shown to be AGAS, as well as LISS with respect to the errors of the KF. Finally, experimental results validated, and demonstrated the goodness of the overall technique, deeming it suitable for real word applications where highly accurate attitude data is a key demand.

A Unit Quaternion Representation

Let $\mathbf{q}(t) \in Q$ denote a unit quaternion with real and imaginary parts denoted by $\tilde{s}(t) \in \mathbb{R}$ and $\tilde{\mathbf{r}}(t) \in \mathbb{R}^3$, respectively, with the group of unit quaternions defined as $Q := \left\{ \mathbf{q} = \begin{bmatrix} \tilde{s} & \tilde{\mathbf{r}}^{\mathsf{T}} \end{bmatrix}^{\mathsf{T}} \mid \mathbf{q}^{\mathsf{T}}\mathbf{q} = 1 \right\}$. Take the representation of $\tilde{\mathbf{R}}(t)$ by means of $\mathbf{q}(t)$, which, in view of the angle-axis representation (31), is given by

$$\tilde{\mathbf{R}}(t) = \mathbf{I} + 2\tilde{s}(t)\mathbf{S}\left[\tilde{\mathbf{r}}(t)\right] + 2\mathbf{S}^2\left[\tilde{\mathbf{r}}(t)\right], \qquad \text{(A.1)}$$

where $\tilde{s}(t) = \cos(\tilde{\theta}(t)/2)$ and $\tilde{\mathbf{r}}(t) = \tilde{\mathbf{v}}(t)\sin(\tilde{\theta}(t)/2)$. Recall the derivative of $\tilde{\mathbf{R}}(t)$, as expressed by (29), and write it as $\dot{\tilde{\mathbf{R}}}(t) = \tilde{\mathbf{R}}(t)\mathbf{S}[\tilde{\boldsymbol{\omega}}(t)]$, with $\tilde{\boldsymbol{\omega}}(t) := \tilde{\boldsymbol{\omega}}_{\boldsymbol{\eta}}(t) + (\mathbf{I} - \tilde{\mathbf{R}}^{\mathsf{T}}(t))^I\boldsymbol{\omega}_E - k_{\boldsymbol{\omega}_E}\mathbf{S}[\tilde{\mathbf{R}}^{\mathsf{T}}(t)^I\boldsymbol{\omega}_E]^I\boldsymbol{\omega}_E - k_{\mathbf{g}}\mathbf{S}[\tilde{\mathbf{R}}^{\mathsf{T}}(t)^I\mathbf{g}]^I\mathbf{g}$, where $\tilde{\boldsymbol{\omega}}_{\boldsymbol{\eta}}(t) = -\hat{\mathbf{R}}(t)\tilde{\mathbf{b}}_{\boldsymbol{\omega}}(t) + k_{\boldsymbol{\omega}_E}\mathbf{S}[\hat{\mathbf{R}}(t)\tilde{\boldsymbol{\omega}}_E(t)]^I\boldsymbol{\omega}_E + k_{\mathbf{g}}\mathbf{S}[\hat{\mathbf{R}}(t)\tilde{\mathbf{g}}(t)]^I\mathbf{g}$. Straightforward algebraic manipulations allow us to show that the dynamics of $\mathbf{q}(t)$ are given, in vector form, by

$$\begin{cases} \dot{\tilde{s}}(t) = -\dfrac{1}{2}\tilde{\mathbf{r}}^{\mathsf{T}}(t)\tilde{\boldsymbol{\omega}}(t) \\ \dot{\tilde{\mathbf{r}}}(t) = \dfrac{1}{2}\left(\tilde{s}(t)\mathbf{I} + \mathbf{S}\left[\tilde{\mathbf{r}}(t)\right]\right)\tilde{\boldsymbol{\omega}}(t) \end{cases}. \tag{A.2}$$

Notice that, from (A.1), one can write $\mathbf{S}[\tilde{\mathbf{R}}^{\mathsf{T}}(t)^I\boldsymbol{\omega}_E]^I\boldsymbol{\omega}_E = 2\tilde{s}(t)\|^I\boldsymbol{\omega}_E\|^2\tilde{\mathbf{r}}(t) - 2(^I\boldsymbol{\omega}_E^{\mathsf{T}}\tilde{\mathbf{r}}(t))(\tilde{s}(t)\mathbf{I} - \mathbf{S}[\tilde{\mathbf{r}}(t)])^I\boldsymbol{\omega}_E$, where a few properties related to the cross product were employed. Further notice the equality $\tilde{\mathbf{R}}(t)\tilde{\mathbf{r}}(t) = \tilde{\mathbf{r}}(t)$. Moreover, $[\mathbf{I} - \tilde{\mathbf{R}}^{\mathsf{T}}(t)]^I\boldsymbol{\omega}_E = 2\left(\tilde{s}(t)\mathbf{I} - \mathbf{S}[\tilde{\mathbf{r}}(t)]\right)\mathbf{S}[\tilde{\mathbf{r}}(t)]^I\boldsymbol{\omega}_E$. Repeating the previous steps for $^I\mathbf{g}$, and substituting in (A.2), the vector part of the quaternion dynamics becomes

$$\begin{aligned} \dot{\tilde{\mathbf{r}}}(t) = &\left(-\mathbf{S}\left[^I\boldsymbol{\omega}_E\right] + k_{\boldsymbol{\omega}_E}\mathbf{S}^2\left[^I\boldsymbol{\omega}_E\right] + k_{\mathbf{g}}\mathbf{S}^2\left[^I\mathbf{g}\right]\right)\tilde{\mathbf{r}}(t) + \\ &+ \gamma(\tilde{\mathbf{r}})\tilde{\mathbf{r}}(t) + \frac{1}{2}\left(\tilde{s}(t)\mathbf{I} + \mathbf{S}\left[\tilde{\mathbf{r}}(t)\right]\right)\tilde{\boldsymbol{\omega}}_{\boldsymbol{\eta}}(t). \end{aligned} \tag{A.3}$$

where $\gamma(\tilde{\mathbf{r}}) = k_{\boldsymbol{\omega}_E}\left\|^I\boldsymbol{\omega}_E \times \tilde{\mathbf{r}}(t)\right\|^2 + k_{\mathbf{g}}\left\|^I\mathbf{g} \times \tilde{\mathbf{r}}(t)\right\|^2$. In turn, the dynamics associated with $\tilde{s}(t)$ follows as

$$\dot{\tilde{s}}(t) = \gamma(\tilde{\mathbf{r}})\tilde{s}(t) - \frac{1}{2}\tilde{\mathbf{r}}^{\mathsf{T}}(t)\tilde{\boldsymbol{\omega}}_{\boldsymbol{\eta}}(t). \tag{A.4}$$

Lemma 5 *Consider $\tilde{\boldsymbol{\omega}}_{\boldsymbol{\eta}}(t) \equiv \mathbf{0}$. Consequently, the 1st-order approximation of the nonlinear differential equation* (A.3) *yields a linear time-invariant (LTI) system that can be expressed as $\dot{\mathbf{z}}(t) = \boldsymbol{\Lambda}\mathbf{z}(t)$, with $\boldsymbol{\Lambda} = (-\mathbf{S}\left[^I\boldsymbol{\omega}_E\right] + k_{\boldsymbol{\omega}_E}\mathbf{S}^2\left[^I\boldsymbol{\omega}_E\right] + k_{\mathbf{g}}\mathbf{S}^2\left[^I\mathbf{g}\right])$. Given* Assumption *1, and $k_{\boldsymbol{\omega}_E} > 0$ and $k_{\mathbf{g}} > 0$, then, for any $\mathbf{c} \in \mathbb{R}^3$, $\mathbf{c} \neq \mathbf{0}$, it follows that $\mathbf{c}^{\mathsf{T}}\boldsymbol{\Lambda}\mathbf{c} = -k_{\boldsymbol{\omega}_E}\left\|^I\boldsymbol{\omega}_E \times \mathbf{c}\right\|^2 - k_{\mathbf{g}}\left\|^I\mathbf{g} \times \mathbf{c}\right\|^2 < 0$. This means that $\boldsymbol{\Lambda}$ is Hurwitz, which suffices to say that the LTI differential equation $\dot{\mathbf{z}}(t) = \boldsymbol{\Lambda}\mathbf{z}(t)$ is exponentially stable, i.e., $\mathbf{z}(t) \to 0$ as $t \to \infty$. Therefore, the system* (29)*, considering unperturbed dynamics, is locally exponentially stable to $\mathbf{I}$.*

References

[1] H. F. Grip, T. I. Fossen, T. A Johansen, and A. Saberi. Globally exponentially stable attitude and gyro bias estimation with application to GNSS/INS integration. *Automatica*, 51:158–166, January 2015.

[2] P. Martin and E. Salaun. Invariant observers for attitude and heading estimation from low-cost inertial and magnetic sensors. In *2007 46th IEEE Conference on Decision and Control*. IEEE, December 2007.

[3] J. F. Guerrero-Castellanos, H. Madrigal-Sastre, S. Durand, L. Torres, and G. A. Muñoz-Hernández. A Robust Nonlinear Observer for Real-Time Attitude Estimation Using Low-Cost MEMS Inertial Sensors. *Sensors*, 13(11):15138–15158, November 2013.

[4] T. Lee, M. Leok, N. H. McClamroch, and A. Sanyal. Global Attitude Estimation using Single Direction Measurements. In *2007 American Control Conference*. IEEE, July 2007.

[5] P. Batista, C. Silvestre, and P. Oliveira. A GES attitude observer with single vector observations. *Automatica*, 48(2):388–395, February 2012.

[6] A. P. Vinod, A. D. Mahindrakar, S. Bandyopadhyay, and V. Muralidharan. A Deterministic Attitude Estimation Using a Single Vector Information and Rate Gyros. *IEEE/ASME Transactions on Mechatronics*, 20(5):2630–2636, October 2015.

[7] H. F. Grip, T. I. Fossen, T. A. Johansen, and A. Saberi. Attitude Estimation Using Biased Gyro and Vector Measurements With Time-Varying Reference Vectors. *IEEE Transactions on Automatic Control*, 57(5):1332–1338, May 2012.

[8] P. Batista, C. Silvestre, and P. Oliveira. Globally exponentially stable cascade observers for attitude estimation. *Control Engineering Practice*, 20(2):148–155, February 2012.

[9] D. Titterton and J. Weston. *Strapdown Inertial Navigation Technology*. Institution of Engineering and Technology, 2004.

[10] A. Albrecht and J. Petereit. Application of an off-the-shelf Fiber Optic Gyroscope based Inertial Measurement Unit for attitude and heading estimation. In *2017 IEEE SENSORS*. IEEE, October 2017.

[11] A. R. Spielvogel and L. L. Whitcomb. Adaptive bias and attitude observer on the special orthogonal group for true-north gyrocompass systems: Theory and preliminary results. *The International Journal of Robotics Research*, page 027836491988168, November 2019.

[12] B. Allotta, R. Costanzi, F. Fanelli, N. Monni, and A. Ridolfi. Single axis FOG aided attitude estimation algorithm for mobile robots. *Mechatronics*, 30:158–173, September 2015.

[13] R. Mahony, T. Hamel, and J.-M. Pflimlin. Nonlinear Complementary Filters on the Special Orthogonal Group. *IEEE Transactions on Automatic Control*, 53(5):1203–1218, June 2008.

[14] P. Batista, C. Silvestre, and P. Oliveira. Globally exponentially stable attitude observer with Earth velocity estimation. *Asian Journal of Control*, 21(4):1409–1422, March 2019.

[15] P. Batista, C. Silvestre, and P. Oliveira. Attitude observer on the special orthogonal group with Earth velocity estimation. *Systems & Control Letters*, 126:33–39, April 2019.

[16] J. Reis, P. Batista, P. Oliveira, and C. Silvestre. Nonlinear Observer on SO(3) for Attitude Estimation on Rotating Earth Using Single Vector Measurements. *IEEE Control Systems Letters*, 3(2):392–397, April 2019.

[17] J. Reis, P. Batista, P. Oliveira, and C. Silvestre. Attitude estimation using high-grade gyroscopes. *Control Engineering Practice*, 92:104134, November 2019.

[18] J. Reis, P. Batista, P. Oliveira, and C. Silvestre. Kalman filter cascade for attitude estimation on rotating Earth. *IEEE/ASME Transactions on Mechatronics*, 2020.

[19] T. Kailath, A. H. Sayed, and B. Hassibi. *Linear Estimation*. Pearson Education (US), 2000.

[20] G. Chang. Alternative formulation of the Kalman filter for correlated process and observation noise. *IET Science, Measurement & Technology*, 8(5):310–318, September 2014.

[21] B. D. O. Anderson. Stability properties of Kalman-Bucy filters. *Journal of the Franklin Institute*, 291(2):137–144, February 1971.

[22] P. Batista, C. Silvestre, and P. Oliveira. On the observability of linear motion quantities in navigation systems. *Systems & Control Letters*, 60(2):101–110, 2011.

[23] M. D. Hua. *Contributions to the automatic control of aerial vehicles*. PhD thesis, Université Nice Sophia Antipolis, 2009.

[24] H. K. Khalil. *Nonlinear Systems*. Prentice Hall, 2nd edition, 2000.

[25] J. Reis, P. Batista, P. Oliveira, and C. Silvestre. Calibration of High-Grade Inertial Measurement Units Using a Rate Table. *IEEE Sensors Letters*, 3(4):1–4, April 2019.